EasyChair Preprint

№ 10312

# A Novel Method for Maneuvering Extended Vehicle Tracking with Automotive Radar

Hongfei Xu, Yaowen Li, Yuxin Ke, Zhizhuo Jiang and Yu Liu



May 31, 2023

# A Novel Method for Maneuvering Extended Vehicle Tracking with Automotive Radar

Hongfei Xu
*Tsinghua Shenzhen International Graduate School*
*Tsinghua University*
Shenzhen, China
xhf21@mails.tsinghua.edu.cn

Yaowen Li
*Tsinghua Shenzhen International Graduate School*
*Tsinghua University*
Shenzhen, China
liyw23@sz.tsinghua.edu.cn

Yuxin Ke
*Tsinghua Shenzhen International Graduate School*
*Tsinghua University*
Shenzhen, China
keyx22@mails.tsinghua.edu.cn

Zhizhuo Jiang
*Tsinghua Shenzhen International Graduate School*
*Tsinghua University*
Shenzhen, China
jiangzhizhuo@sz.tsinghua.edu.cn

Yu Liu
*Department of Electronic Engineering*
*Tsinghua University*
Beijing, China
liuyu77360132@126.com

***Abstract*—In high-resolution automotive radar tracking systems, vehicle targets are often regarded as extended targets, which means multiple measurements originated from scattering centers of vehicle targets can be detected at each scan and thus the traditional point target tracking schemes are unsuitable. Meanwhile, vehicle maneuvers, e.g., braking and swerving, cause serious degradation of the classical extended target tracking methods. In this paper, a novel method is proposed for maneuvering extended vehicle tracking with automotive radar. The data-region association (DRA) strategy is adopted to handle the vehicle extension effect, which is superior in describing the complex spatial distribution of vehicle target measurements. The interacting multiple model (IMM) method is combined with this DRA strategy to describe the evolution of target motion models. Accordingly, the proposed DRA-IMM method achieves satisfying tracking performance of extended vehicles and also guarantees the robustness in case of maneuvers. Furthermore, in view of the correlation between vehicle extension and its kinematic state, a ray-based strategy is devised to improve the prior distribution of the data-region association of the basic DRA-IMM, and accordingly an enhanced DRA-IMM (EDRA-IMM) method is proposed. Simulation result validates the effectiveness of the proposed DRA-IMM method for maneuvering extended vehicle tracking and the further improvement of the proposed EDRA-IMM method.**

***Index Terms*—Automotive radar, extended target tracking, maneuvering target tracking, data-region association, interactive multiple model**

## I. Introduction

Automotive radar has been recognized as a powerful sensor in the intelligent transportation application. Nowadays, advanced automotive radars are devised for increasingly high resolutions and enabled to capture multiple scattering centers of vehicle targets. In this context, the traditional point target tracking schemes are inadequate, while the extended target tracking (ETT) algorithms, capable of estimating the shapes apart from the kinematic states of vehicles, become more and more popular [1]–[5].

Representative methods for ETT are summarized as follows. The random matrix model (RMM) is developed to describe the elliptical extension pattern of targets [1], [2]. Another prevalent method is the random hypersurface model (RHM) which can describe other extension patterns [3], [4]. Note that these traditional ETT solutions simply assume that the measurements are uniformly distributed over the entire extension, which may be violated and much more complex in practice. For example, the rear of a vehicle is more likely to be detected than the other regions when the radar trailed behind, but so is the right region when this vehicle turns right.

To depict the complex spatial distribution of measurements over vehicle extension, a data-region association (DRA) method is proposed for automotive radar tracking [5]. The DRA method partitions the rectangle extension of vehicles into five regions, each of which represents a cluster of scattering centers and corresponds to an individual component of the spatial distribution of measurements. This division strategy is more reasonable and superior to uniform distribution assumption of the RMM and the RHM methods since radar measurements of a vehicle mainly originate from its boundary close to the radar as well as the headlamps and the wheel housings [6]. However, the standard DRA assumes that the vehicle moves according to a certain motion model, resulting in serious degradation of tracking performance of maneuvering vehicles.

Vehicle maneuver is another challenge to automotive radar tracking [7]–[9]. The existing algorithms for maneuvering target tracking can be categorized as single-model and multiple-model schemes. Comprehensive reviews of these algorithms are presented in [10]–[14]. Among these algorithms, the

interacting multiple model (IMM) [15] is preferred due to the reasonable balance between tracking accuracy of maneuvering targets and complexity [16]. The IMM is a suboptimal hybrid filter that holds several dynamic hypotheses simultaneously and is verified to be a cost-effective hybrid state estimation scheme [13]. However, the IMM is proposed for point target tracking and not suitable for ETT, especially for vehicle measurements subject to complex spatial distributions.

In this paper, we propose a novel method integrating the standard DRA with the IMM, referred to as the DRA-IMM. In this method, the standard DRA strategy is adopted to depict the complex spatial distribution of extended vehicle target measurements. Then the IMM method is combined with the DRA strategy to describe the evolution of target motion models. Accordingly, the proposed DRA-IMM not only achieves satisfying tracking performance of extended vehicles, but also guarantees the robustness in case of maneuvers.

Furthermore, an enhanced DRA-IMM (EDRA-IMM) is proposed to overcome the drawback that the basic DRA-IMM uses a constant prior probability of data-region association and ignores the temporal variation of vehicle extension with kinematic state. A ray-based strategy is devised to depict the correlation between vehicle extension and its kinematic state, and adaptively adjust the prior probability of data-region association to vehicle maneuvers. Hence, the proposed EDRA-IMM further improves the vehicle tracking accuracy compared with the basic DRA-IMM, especially in the maneuvering phase.

Simulation results of vehicle tracking validates the significant superiority in robustness of the proposed DRA-IMM over the standard DRA in case of sharp maneuvers. Moreover, the proposed EDRA-IMM further reduces the tracking error compared with the basic DRA-IMM, especially when the vehicle maneuvers and exhibits time-varying extension effect.

## II. System Model

The system model is defined on the following three coordinate systems: The global Cartesian coordinate system $O_{\mathrm{G}}-x_{\mathrm{G}}y_{\mathrm{G}}$ in which the states of the target, radar, and ego vehicle are defined, the target Cartesian coordinate system $O_{\mathrm{T}}-x_{\mathrm{T}}y_{\mathrm{T}}$ which is used to describe the spatial distribution of measurements and the radar polar coordinate system $O_{\mathrm{S}}-x_{\mathrm{S}}y_{\mathrm{S}}$ (see Fig. 1).

### A. Target Dynamic Model

The target motion model is defined as:

$$\boldsymbol{x}_k = \mathbf{F}_{k-1}\boldsymbol{x}_{k-1} + \mathbf{G}_{k-1}\boldsymbol{w}_{k-1}, \tag{1}$$

where $\boldsymbol{x}_k$ is the state vector and $\mathbf{F}_{k-1}$ is the state transition matrix; $\boldsymbol{w}_k$ denotes the zero-mean white Gaussian process noise with the following covariance matrix $\mathbf{Q}_k$ and coefficient matrix $\mathbf{G}_k$:

$$\mathbf{Q}_k = \mathrm{cov}\left([w_x, w_y, w_\omega, \boldsymbol{w}_{\boldsymbol{p}}]^T\right) = \mathrm{diag}([\sigma_x, \sigma_y, \sigma_\omega, \sigma_p \boldsymbol{I}_4]) \tag{2}$$

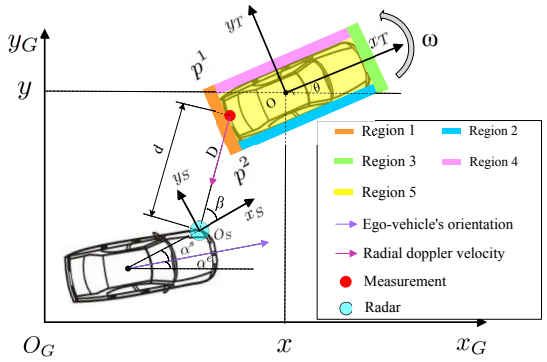


Fig. 1. Illustration of the data-region association concept. Regions 1-5 correspond to the five clusters of scattering centers over the vehicle extension. $\boldsymbol{p}^1$ and $\boldsymbol{p}^2$ are the vertices of the rectangle extension. $\alpha^e$ is the ego-vehicle's orientation. $\alpha^s$ is the angle between the ego-vehicle's orientation and the radar's boresight that is known.

$$\begin{aligned} \mathbf{G}_k &= \mathrm{diag}\left(\mathbf{G}^c, \mathbf{G}^c, 1, \mathbf{I}_4\right) \\ \mathbf{G}^c &= \left[T^2/2, T, 1\right]^{\mathrm{T}}, \end{aligned} \tag{3}$$

where $\mathbf{I}_n$ is the $n \times n$ identity matrix, $\mathrm{cov}(\cdot)$ represents covariance operator and $\mathrm{diag}(\cdot)$ represents a diagonal matrix. Note that $\mathbf{G}_k$ is an $11 \times 7$ matrix, $\mathbf{Q}_k$ is a $7 \times 7$ matrix and $\boldsymbol{w}_k$ is a $7 \times 1$ vector.

The state vector $\boldsymbol{x}_k$ is defined as:

$$\boldsymbol{x}_k = \left[x_k, \dot{x}_k, \ddot{x}_k, y_k, \dot{y}_k, \ddot{y}_k, \omega_k, \left(\boldsymbol{p}_k^1\right)^{\mathrm{T}}, \left(\boldsymbol{p}_k^2\right)^{\mathrm{T}}\right]^{\mathrm{T}} \tag{4}$$

Here $(x_k, y_k)^{\mathrm{T}}$, $(\dot{x}_k, \dot{y}_k)^{\mathrm{T}}$, $(\ddot{x}_k, \ddot{y}_k)^{\mathrm{T}}$, and $\omega_k$ denote the position, velocity, acceleration, and yaw rate of the target centroid, respectively. To handle vehicle maneuvers, the IMM algorithm is employed, consisting the constant-velocity (CV) model, the constant-acceleration (CA) model and the coordinated-turn (CT) model. Note that in the CV model, $\ddot{x}_k = \ddot{y}_k = \omega_k = 0$. Similarly, $\omega_k = 0$ in the CA model and $\ddot{x}_k = \ddot{y}_k = 0$ in the CT model. $\boldsymbol{p}_k^1$ and $\boldsymbol{p}_k^2$ are the vertices of the rectangle extension (see Fig. 1). Here $\boldsymbol{p}_k^1$ or $\boldsymbol{p}_k^2$ is a vector of two values each referring to $x$ and $y$ coordinates of the vertice in the target Cartesian coordinate system. Clearly, the other two vertices $\boldsymbol{p}_k^3$ and $\boldsymbol{p}_k^4$ shown in Fig. 2 can be represented by $-\boldsymbol{p}_k^1$ and $-\boldsymbol{p}_k^2$ in the same coordinate system. So $\boldsymbol{p}_k^1$ and $\boldsymbol{p}_k^2$ suffice to describe the rectangle extension.

Particularly, $\mathbf{F}_k$ is defined as [5]

$$\mathbf{F}_k = \mathrm{diag}\left(\bar{\mathbf{F}}_k, \mathbf{F}_k^s\right), \tag{5}$$

where $\bar{\mathbf{F}}_k$ denotes the kinematic state transition matrices and $\mathbf{F}_k^s$ is the extension state transition matrix as defined in [5]. Although the exact forms of transition matrices are distinct in CV,CA and CT models which can be found in [17], [18], they are uniformly characterized by the same symbol for simplicity.

### B. Measurement Model

Suppose that an extended target generates $N_k$ measurements, represented by a stack vector at time $k$:

$$\boldsymbol{Z}_k = \left[\left(\boldsymbol{z}_k^1\right)^{\mathrm{T}}, \left(\boldsymbol{z}_k^2\right)^{\mathrm{T}}, \ldots, \left(\boldsymbol{z}_k^{N_k}\right)^{\mathrm{T}}\right]^{\mathrm{T}}. \tag{6}$$

Here $\boldsymbol{z}_k^r = [d_k^r, D_k^r, \beta_k^r]^{\mathrm{T}} (r = 1, \ldots, N_k)$ contains the distance $d$, the radial Doppler velocity $D$, and the azimuth angle $\beta$ in the radar polar coordinate, as shown in Fig. 1.

The measurement model of the DRA strategy is stated as follows [19]:

$$\begin{aligned}\boldsymbol{z}_k^r &= \begin{bmatrix} \|\mathbf{H}_i \boldsymbol{x}_k - \boldsymbol{p}_k^s\| + v_{d,k}^r \\ \frac{(\mathbf{A}_3 \boldsymbol{x}_k + (\boldsymbol{A}_4 \boldsymbol{x}_k)\mathbf{A}_1 (\mathbf{H}_i - \mathbf{A}_2)\boldsymbol{x}_k - \boldsymbol{D}_k^s)^{\mathrm{T}} (\mathbf{H}_i \boldsymbol{x}_k - \boldsymbol{p}_k^s)}{\|\mathbf{H}_i \boldsymbol{x}_k - \boldsymbol{p}_k^s\|} + v_{D,k}^r \\ (\angle (\mathbf{H}_i \boldsymbol{x}_k - \boldsymbol{p}_k^s)) - \alpha^s - \alpha_k^e + v_{\beta,k}^r \end{bmatrix} \\ &= \boldsymbol{h}_i^r (\boldsymbol{x}_k, \boldsymbol{\zeta}_k^r, \boldsymbol{v}_k^r), \end{aligned} \tag{7}$$

where $\boldsymbol{p}_k^s$ and $\boldsymbol{D}_k^s$ are the position and velocity of the radar and $\boldsymbol{v}_k^r = [v_{d,k}^r, v_{D,k}^r, v_{\beta,k}^r]$ is Gaussian noise. $\mathbf{H}_i$ is a function of $\boldsymbol{\zeta}_k^r$. Since the extension is divided into five regions (Fig. 1), $i$ in $\mathbf{H}_i$ and $\boldsymbol{h}_i^r$ represents the index of the region ranging from 1 to 5. Then $\boldsymbol{\zeta}_k^r = [s_k^r, 0]$ if $i < 5$ and $\boldsymbol{\zeta}_k^r = [s_k^{r_1}, s_k^{r_2}]$ if $i = 5$. Specifically [5],

$$\mathbf{H}_1 = [\mathbf{A}_5, s_k^r \mathbf{I}_2, (1 - s_k^r)\mathbf{I}_2] \tag{8}$$

$$\mathbf{H}_2 = [\mathbf{A}_5, (s_k^r - 1)\mathbf{I}_2, s_k^r \mathbf{I}_2] \tag{9}$$

$$\mathbf{H}_3 = [\mathbf{A}_5, -s_k^r \mathbf{I}_2, (s_k^r - 1)\mathbf{I}_2] \tag{10}$$

$$\mathbf{H}_4 = [\mathbf{A}_5, (1 - s_k^r)\mathbf{I}_2, -s_k^r \mathbf{I}_2] \tag{11}$$

$$\mathbf{H}_5 = [\mathbf{A}_5, (1 - s_k^{r_1} - s_k^{r_2})\mathbf{I}_2, (s_k^{r_1} - s_k^{r_2})\mathbf{I}_2]. \tag{12}$$

Here, $s_k^r$ (or $s_k^{r_1}, s_k^{r_2}$) represents a uniform distribution variable over $[0, 1]$ which means the scattering centers are uniformly distributed in each region. In (7)-(12), $\mathbf{A}_1 = \left[[0,1]^{\mathrm{T}}, [-1,0]^{\mathrm{T}}\right]$, $\mathbf{A}_2 = [\mathbf{A}_5, \mathbf{0}_{2\times 4}]$, $\mathbf{A}_3 = \left[\boldsymbol{e}_9^2, \boldsymbol{e}_9^4\right]^{\mathrm{T}}$, $\boldsymbol{A}_4 = \left(\boldsymbol{e}_9^5\right)^{\mathrm{T}}$, $\mathbf{A}_5 = \left[\boldsymbol{e}_5^1, \boldsymbol{e}_5^3\right]^{\mathrm{T}}$, where $\mathbf{0}_{n\times m}$ represents $n \times m$ zero matrix and $\boldsymbol{e}_n^i = [0, \cdots, 0, 1, 0, \cdots, 0]^{\mathrm{T}}$ denotes the $n$-dimensional base vector of all zeros except the $i$-th element being one.

## III. The Proposed Method

In this section, the DRA-IMM method is first presented. Then, based on that, the EDRA-IMM method is proposed by incorporating the estimated kinematic state information to improve the calculation of the prior data-region association probability.

### A. The proposed DRA-IMM method

*1) The posterior estimation formulation:*

The proposed DRA-IMM method has a recursive estimation scheme. At the $k$-th scan, the posterior state estimate of the proposed DRA-IMM method is calculated by

$$\hat{\boldsymbol{x}}_{k|k} = \sum_{j=1}^{3} \left[ \sum_{\eta=1}^{m_k} \hat{\boldsymbol{x}}_{k|k}^{\eta,j} P_\varphi \left( \boldsymbol{\varphi}_k^\eta \mid \boldsymbol{Z}^k, u_k^j \right) \right] P_u \left( u_k^j \mid \boldsymbol{Z}^k \right), \tag{13}$$

where $\boldsymbol{\varphi}_k^\eta$ is the $\eta$-th data-region association hypothesis of all $m_k$ hypotheses. Specifically, given $N_k$ measurements, there are $m_k = 5^{N_k}$ association hypotheses and $m_k$ is likewise quite large for large N. To reduce computation, five rectangle gates covering the corresponding regions are used for data-region association. For instance, in Fig. 2 there are two measurements

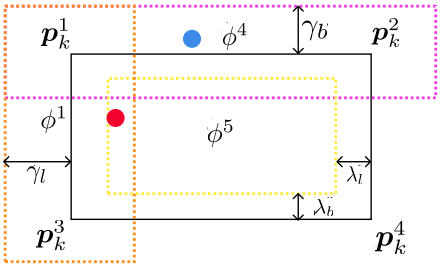


Fig. 2. Illustration of gating and data-region association. Only the region 1, 4 and 5 ($\phi^1, \phi^4$ and $\phi^5$) are displayed, and the same size of gates applies to the region 2 and 3. The blue and red circles are the two measurements. $\gamma_l$ and $\gamma_b$ determine the size of gates for sides while $\lambda_l$ and $\lambda_b$ determine the gates for interior. They can be calculated by $\gamma_l = t\left(\hat{p}_{k|k-1}^1 - \hat{p}_{k|k-1}^4\right)$, $\gamma_b = t\left(\hat{p}_{k|k-1}^1 - \hat{p}_{k|k-1}^2\right)$, $\lambda_l = \tilde{t}\left(\hat{p}_{k|k-1}^1 - \hat{p}_{k|k-1}^4\right)$, $\lambda_b = \tilde{t}\left(\hat{p}_{k|k-1}^1 - \hat{p}_{k|k-1}^2\right)$ with predetermined scaling factors $t$ and $\tilde{t}$, where $\hat{p}_{k|k-1}^v (v = 1, ..., 4)$ can be calculated by (1).

at the $k$-th scan. After gating, one of the measurements only falls within the gate of region 4, while the other simultaneously falls within the gates of region 1 and region 5, resulting in two association hypotheses: $\varphi^1 = \{\phi^4, \phi^1\}$ and $\varphi^2 = \{\phi^4, \phi^5\}$. In this case, $\eta = 1$ or 2. Particularly, if the measurement is not inside any gate, it is associated with the nearest side.

In (13), $u_k^j$ ($j = 1, 2, 3$ for the CV, CA and CT models) is the motion model, and $\boldsymbol{Z}^k$ is the measurements over the previous $k$ scans; $\hat{\boldsymbol{x}}_{k|k}^{\eta,j}$ is the posterior estimation conditioned on $\boldsymbol{\varphi}_k^\eta$ and $u_k^j$. $P_\varphi\left(\boldsymbol{\varphi}_k^\eta \mid \boldsymbol{Z}^k, u_k^j\right)$ is the data-region association probability given the motion model $u_k^j$, which can be calculated by the DRA method. $P_u\left(u_k^j \mid Z^k\right)$ is the motion model probability which is updated by the IMM.

*2) The DRA update:*

Given the motion model $u_k^j$, the data-region association probability in (13) is calculated by

$$\begin{aligned} P_\varphi\left(\boldsymbol{\varphi}_k^\eta \mid \boldsymbol{Z}^k, u_k^j\right) &= p\left(\boldsymbol{Z}_k \mid \boldsymbol{\varphi}_k^\eta, u_k^j, \boldsymbol{Z}^{k-1}\right) \\ &\quad \cdot P_\varphi\left(\boldsymbol{\varphi}_k^\eta \mid u_k^j, \boldsymbol{Z}^{k-1}\right) \Big/ c_1 \end{aligned} \tag{14}$$

$$c_1 = \sum_{\eta=1}^{m_k} p\left(\boldsymbol{Z}_k \mid \boldsymbol{\varphi}_k^\eta, u_k^j, \boldsymbol{Z}^{k-1}\right) \cdot P_\varphi\left(\boldsymbol{\varphi}_k^\eta \mid u_k^j, \boldsymbol{Z}^{k-1}\right), \tag{15}$$

where the prior data-region association probability $P_\varphi\left(\boldsymbol{\varphi}_k^\eta \mid u_k^j, \boldsymbol{Z}^{k-1}\right)$ given $u_k^j$ is assumed as [5]

$$P_\varphi\left(\boldsymbol{\varphi}_k^\eta \mid u_k^j, \boldsymbol{Z}^{k-1}\right) = \frac{1}{m_k}, \eta = 1, \ldots, m_k, \tag{16}$$

and $p\left(\boldsymbol{Z}_k \mid \boldsymbol{\varphi}_k^\eta, u_k^j, \boldsymbol{Z}^{k-1}\right)$ is the likelihood of measurements given $\boldsymbol{\varphi}_k^\eta$ and $u_k^j$, satisfying

$$p\left(\boldsymbol{Z}_k \mid \boldsymbol{\varphi}_k^\eta, u_k^j, \boldsymbol{Z}^{k-1}\right) = \mathcal{N}\left(\boldsymbol{Z}_k; \hat{\boldsymbol{Z}}_k^{\eta,j}, \mathbf{S}_k^{\eta,j}\right), \tag{17}$$

where $\hat{\boldsymbol{Z}}_k^{\eta,j}$ is measurement prediction whose covariance is $\mathbf{S}_k^{\eta,j}$. Note that (14)-(17) are similar to the DRA formulations

in [5]. However, the proposed DRA-IMM method incorporates the IMM strategy in the basic DRA framework to handle vehicle maneuvers, and thus (14)-(17) are reformulated under the condition of the motion model $u_k^j$, as defined in (13).

The unscented transformation (UT) [20] is utilized to estimate $\hat{\boldsymbol{Z}}_k^{\eta,j}$ and $\mathbf{S}_k^{\eta,j}$. Given $\boldsymbol{\varphi}_k^{\eta}$ and $u_k^j$, the measurement model is

$$\begin{aligned}\boldsymbol{Z}_k &= \left[\left(\boldsymbol{z}_k^1\right)^{\mathrm{T}},\ldots,\left(\boldsymbol{z}_k^{N_k}\right)^{\mathrm{T}}\right]^{\mathrm{T}} = \left[\left(\boldsymbol{h}_i^1\right)^{\mathrm{T}},\ldots,\left(\boldsymbol{h}_i^{N_k}\right)^{\mathrm{T}}\right]^{\mathrm{T}} \\ &= \check{\boldsymbol{h}}\left(\boldsymbol{x}_k,\boldsymbol{\zeta}_k^1,\ldots,\boldsymbol{\zeta}_k^{N_k},\boldsymbol{v}_k^1,\ldots,\boldsymbol{v}_k^{N_k}\right),\end{aligned} \tag{18}$$

where $\boldsymbol{h}_i^r$ $(i=1,\ldots,5)$ is the measurement model for $\boldsymbol{z}_k^r$ defined in (7) and $\check{\boldsymbol{h}}$ is the overall measurement model. To estimate $\hat{\boldsymbol{Z}}_k^{\eta,j}$ and $\mathbf{S}_k^{\eta,j}$, the state vector is augmented by

$$\boldsymbol{x}_k^{\eta,j,A} \triangleq \left[(\boldsymbol{x}_k^{\eta,j})^{\mathrm{T}},\boldsymbol{\zeta}_k^1,\ldots,\boldsymbol{\zeta}_k^{N_k},\boldsymbol{v}_k^1,\ldots,\boldsymbol{v}_k^{N_k}\right]^{\mathrm{T}}. \tag{19}$$

Then we have

$$\left(\hat{\boldsymbol{Z}}_k^{\eta},\mathbf{S}_k^{\eta}\right) = \mathrm{UT}\left[\check{h}\left(\boldsymbol{x}_k^{\eta,j,A}\right),\hat{\boldsymbol{x}}_{k|k-1}^{\eta,j,A},\mathbf{P}_{k|k-1}^{\eta,j,A}\right], \tag{20}$$

where UT means the unscented transformation with sample points $\left\{\check{\boldsymbol{h}}\left(\boldsymbol{x}_k^{\eta,j,A,l}\right)\right\}$ weighted by $\{\delta_l\}, l=1,\ldots,\tilde{N}$ and $\boldsymbol{x}_k^{\eta,j,A,l}$ is the $l$th sample point of $\boldsymbol{x}_k^{\eta,j,A}$. From (14)-(20), the data-region association probability can be obtained.

The posterior estimation $\hat{\boldsymbol{x}}_{k|k}^{\eta,j}$ conditioned on $\boldsymbol{\varphi}_k^{\eta}$ and $u_k^j$ in (13) is calculated by two steps of the unscented filtering including prediction and update. The predicted state in (20) is calculated by

$$\hat{\boldsymbol{x}}_{k|k-1}^{\eta,j} = \mathbf{F}_{k-1}\tilde{\boldsymbol{x}}_{k-1|k-1}^{j} \tag{21}$$

$$\mathbf{P}_{k|k-1}^{\eta,j} = \mathbf{F}_{k-1}\tilde{\mathbf{P}}_{k-1|k-1}^{j}\mathbf{F}_{k-1}^{\mathrm{T}} + \mathbf{G}_{k-1}\mathbf{Q}_{k-1}\mathbf{G}_{k-1}^{\mathrm{T}}, \tag{22}$$

where the mixed state $\tilde{\boldsymbol{x}}_{k-1|k-1}^{j}$ and $\tilde{\mathbf{P}}_{k-1|k-1}^{j}$ are elaborated in Section III-A3, $\mathbf{G}_{k-1}$ and $\mathbf{Q}_{k-1}$ are defined in Section II-A. And then the state estimation can be updated by

$$\hat{\boldsymbol{x}}_{k|k}^{\eta,j} = \hat{\boldsymbol{x}}_{k|k-1}^{\eta,j} + \mathbf{K}_k^{\eta,j}\left(\boldsymbol{Z}_k - \hat{\boldsymbol{Z}}_k^{\eta,j}\right) \tag{23}$$

$$\mathbf{P}_{k|k}^{\eta,j} = \mathbf{P}_{k|k-1}^{\eta,j} - \mathbf{K}_k^{\eta,j}\mathbf{S}_k^{\eta,j}\left(\mathbf{K}_k^{\eta,j}\right)^{\mathrm{T}}, \tag{24}$$

where the gain $\mathbf{K}_k^{\eta,j}$ is

$$\mathbf{K}_k^{\eta,j} = \mathbf{C}_{\boldsymbol{xz}}^{\eta,j}\left(\mathbf{S}_k^{\eta,j}\right)^{-1} \tag{25}$$

$$\mathbf{C}_{\boldsymbol{xz}}^{\eta,j} = \sum_{l=1}^{\tilde{N}}\delta_l\left[\boldsymbol{x}_k^l - \hat{\boldsymbol{x}}_{k|k-1}\right]\left[\check{\boldsymbol{h}}\left(\boldsymbol{x}_k^{A,l}\right) - \hat{\boldsymbol{Z}}_k^{\eta}\right]^{\mathrm{T}}. \tag{26}$$

Eventually, the posterior state estimate under $u_k^j$ is

$$\hat{\boldsymbol{x}}_{k|k}^{j} = \sum_{\eta=1}^{m_k}\hat{\boldsymbol{x}}_{k|k}^{\eta,j}P_{\varphi}\left(\boldsymbol{\varphi}_k^{\eta} \mid \boldsymbol{Z}^k,u_k^j\right) \tag{27}$$

$$\begin{aligned}\mathbf{P}_{k|k}^{j} =& \sum_{\eta=1}^{m_k}P_{\varphi}\left(\boldsymbol{\varphi}_k^{\eta} \mid \boldsymbol{Z}^k,u_k^j\right) \\ &\left[\mathbf{P}_{k|k}^{\eta,j} + \left(\hat{\boldsymbol{x}}_{k|k}^{\eta,j} - \hat{\boldsymbol{x}}_{k|k}^{j}\right)\left(\hat{\boldsymbol{x}}_{k|k}^{\eta,j} - \hat{\boldsymbol{x}}_{k|k}^{j}\right)^{\mathrm{T}}\right].\end{aligned} \tag{28}$$

*3) The IMM update:*

The mixed state conditioned on $\boldsymbol{\varphi}_k^{\eta}$ and $u_k^j$ in (21) and (22) are calculated by interacting the estimated states of the multiple motion models [15], namely:

$$\tilde{\boldsymbol{x}}_{k-1|k-1}^{j} = \sum_{i=1}^{3}\hat{\boldsymbol{x}}_{k-1|k-1}^{i}\boldsymbol{\pi}_{ij}\mu_{k-1}^{i}\Big/\sum_{i=1}^{3}\boldsymbol{\pi}_{ij}\mu_{k-1}^{i} \tag{29}$$

$$\begin{aligned}\tilde{\mathbf{P}}_{k-1|k-1}^{j} =& \Big\{\sum_{i=1}^{3}\Big[\mathbf{P}_{k-1|k-1}^{i} + \left(\hat{\boldsymbol{x}}_{k-1|k-1}^{i} - \tilde{\boldsymbol{x}}_{k-1|k-1}^{j}\right) \\ &\left(\hat{\boldsymbol{x}}_{k-1|k-1}^{i} - \tilde{\boldsymbol{x}}_{k-1|k-1}^{j}\right)^{\mathrm{T}}\Big]\Big\}\boldsymbol{\pi}_{ij}\mu_{k-1}^{i}\Big/\sum_{i=1}^{3}\boldsymbol{\pi}_{ij}\mu_{k-1}^{i},\end{aligned} \tag{30}$$

where $\boldsymbol{\pi}_{ij}$ is the transition probability from motion model $i$ to $j$ and $\mu_{k-1}^{i}$ is the motion model probability estimated at time $k-1$. Then the motion model probability is updated by

$$P_u\left(u_k^j \mid \boldsymbol{Z}^k\right) = P_u\left(u_k^j \mid \boldsymbol{Z}^{k-1}\right)\cdot c_1\Big/c_2 \tag{31}$$

$$c_2 = \sum_{j=1}^{3}P_u\left(u_k^j \mid \boldsymbol{Z}^{k-1}\right)\cdot p\left(\boldsymbol{Z}_k \mid u_k^j,\boldsymbol{Z}^{k-1}\right), \tag{32}$$

where $P_u\left(u_k^j \mid \boldsymbol{Z}^{k-1}\right)$ is the prior motion model probability that can be obtained by $\left\{\mu_{k-1}^{i}\right\}_{i=1}^{3}$ and $\boldsymbol{\pi}_{ij}$ [15]:

$$P_u\left(u_k^j \mid \boldsymbol{Z}^{k-1}\right) = \sum_{i=1}^{3}\boldsymbol{\pi}_{ij}\mu_{k-1}^{i}, \tag{33}$$

and $p\left(\boldsymbol{Z}_k \mid u_k^j,\boldsymbol{Z}^{k-1}\right)$ can be calculated by (15).

Based on the above DRA update and IMM update steps, the posterior state estimate of the proposed DRA-IMM method is obtained as (13):

$$\hat{\boldsymbol{x}}_{k|k} = \sum_{j=1}^{3}\hat{\boldsymbol{x}}_{k|k}^{j}P_u\left(u_k^j \mid \boldsymbol{Z}^k\right) \tag{34}$$

$$\begin{aligned}\mathbf{P}_{k|k} =& \sum_{j=1}^{3}P_u\left(u_k^j \mid \boldsymbol{Z}^k\right) \\ &\left[\mathbf{P}_{k|k}^{j} + \left(\hat{\boldsymbol{x}}_{k|k}^{j} - \hat{\boldsymbol{x}}_{k|k}\right)\left(\hat{\boldsymbol{x}}_{k|k}^{j} - \hat{\boldsymbol{x}}_{k|k}\right)^{\mathrm{T}}\right].\end{aligned} \tag{35}$$

In this way, the proposed DRA-IMM can estimate the state iteratively.

### *B. The proposed EDRA-IMM method*

The proposed DRA-IMM in the previous section assumes that the prior data-region association probabilities given the different motion models are equal and constant in (16). In fact, this prior data-region association probability is closely related to the relative position and attitude between the target and the radar, and varies with the target motion model. For example, if the car turns right in front of the radar, the probability of capturing the right side of the vehicle increases.

Therefore, we propose the EDRA-IMM method and revise the prior data-region association probability in (16) as:

$$P_{\varphi}\left(\boldsymbol{\varphi}_k^{\eta} \mid u_k^j, \boldsymbol{Z}^{k-1}\right) = P_{\varphi}\left(\phi_k^{\eta,1}, \ldots, \phi_k^{\eta,N_k} \mid u_k^j, \boldsymbol{Z}^{k-1}\right) \Big/ c_3, \tag{36}$$

where $c_3$ is the normalization factor as follows

$$c_3 = \sum_{\eta=1}^{m_k} P_{\varphi}\left(\boldsymbol{\varphi}_k^{\eta} \mid u_k^j, \boldsymbol{Z}^{k-1}\right), \tag{37}$$

and $\phi_k^{\eta,i}(i = 1, \ldots, N_k)$ is the region to which the $i$-th measurement is associated in the $\eta$-th data-region association hypothesis as depicted in Fig. 2. Assume that each measurement is generated independently, (36) can be derived as

$$P_{\varphi}\left(\boldsymbol{\varphi}_k^{\eta} \mid u_k^j, \boldsymbol{Z}^{k-1}\right) = P_{\varphi}\left(\phi_k^{\eta,1} \mid u_k^j, \boldsymbol{Z}^{k-1}\right) \cdot P_{\varphi}\left(\phi_k^{\eta,2} \mid u_k^j, \boldsymbol{Z}^{k-1}\right) \cdots P_{\varphi}\left(\phi_k^{\eta,N_k} \mid u_k^j, \boldsymbol{Z}^{k-1}\right) \Big/ c_3. \tag{38}$$

Inspired by [21], we propose a ray-based strategy to calculate $P_{\varphi}\left(\phi_k^{\eta,i} \mid u_k^j, \boldsymbol{Z}^{k-1}\right)$, as shown in Fig. 3. If the associated region $\phi_k^{\eta,i}$ is in the line of sight of radar, then

$$P_{\varphi}\left(\phi_k^{\eta,i} \mid u_k^j, \boldsymbol{Z}^{k-1}\right) = P_{\text{near}} \cdot \left(\frac{\theta_{\text{near}}}{\theta_{\text{near}} + \theta'_{\text{near}}}\right), \tag{39}$$

otherwise,

$$P_{\varphi}\left(\phi_k^{\eta,i} \mid u_k^j, \boldsymbol{Z}^{k-1}\right) = P_{\text{far}} \cdot \left(\frac{\theta_{\text{far}}}{\theta_{\text{far}} + \theta'_{\text{far}}}\right), \tag{40}$$

where $P_{\text{near}}$ and $P_{\text{far}}$, along with the interior part $P_{\text{interior}}$, are the pre-defined probabilities referring to [5], satisfying

$$P_{\text{near}} + P_{\text{far}} + P_{\text{interior}} = 1. \tag{41}$$

The definitions of $\theta_{\text{near}}$, $\theta'_{\text{near}}$, $\theta_{\text{far}}$, and $\theta'_{\text{far}}$ based on the vertices of the rectangular extension are illustrated in Fig. 3, while these vertices can be obtained from the predicted states in (21) of the most likely motion model in the IMM scheme. In this way, $P\left(\phi_k^{\eta,i} \mid u_k^j, \boldsymbol{Z}^{k-1}\right)$ is updated in real time and in accordance with the estimated kinematic state.

From (36)-(41), the prior knowledge of the data-region association probability can be extracted from the estimated kinematic state. Hence, the proposed EDRA-IMM further improves the calculation of the prior data-region association probability over the proposed DRA-IMM.

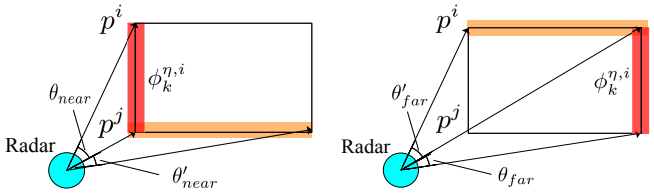


(a) $\phi_k^{\eta,i}$ is in the line-of-sight region (b) $\phi_k^{\eta,i}$ is in the non-line-of-sight region

Fig. 3. Visualization of the ray-based strategy to calculate $P_{\varphi}\left(\phi_k^{\eta,i} \mid u_k^j, \boldsymbol{Z}^{k-1}\right)$.

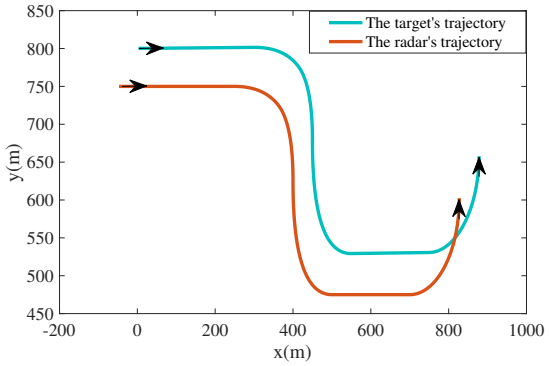


Fig. 4. Trajectories of the target vehicle and the radar.

TABLE I
TARGET ACCELERATION TABLE

| **Maneuvering time (s)** | **10** | **15** | **20** | **30** | **40** |
|---|---|---|---|---|---|
| **X-Acceleration ($m/s^2$)** | -3 | -3 | 2 | 0 | 0 |
| **Y-Acceleration ($m/s^2$)** | -2 | -4 | 3 | 0 | 0 |
| **Yaw rate ($rad/s$)** | 0 | 0 | 0 | 0 | $\pi/20$ |

## IV. EVALUATION

In this section, a $4.8m \times 1.8m$ maneuvering car is tracked, as shown in Fig. 4. The trajectory of the target begins at $(0m, 800m)$ at a speed of $30m/s$ and moves for 50 seconds with the acceleration and yaw rate changing at certain time. The maneuvering acceleration table is shown in Table I. The acceleration keeps constant until the next maneuvering time. Note that the trajectory of the radar is not the same as that of the target, since the noise is different. In the simulation,

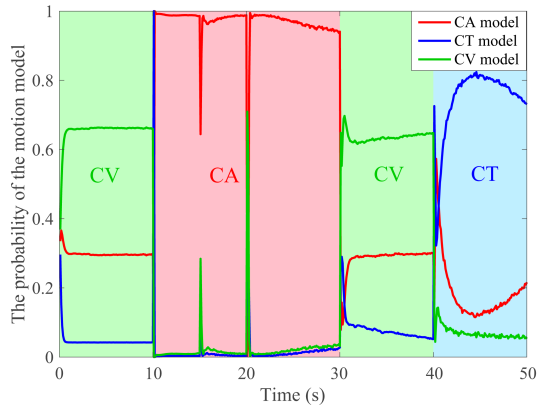


Fig. 5. The estimated probabilities of the CV, CA and CT models of the proposed DRA-IMM method. The ground truth of target motion model is represented by the background color. The proposed method achieves satisfying estimation of the target motion models.

there are $N_k = \bar{N}_k + 1$ measurements at time k, where $\bar{N}_k$ follows Poisson distribution with mean 5. A measurement is a scattering center perturbed by Gaussian noise. The spatial distribution of scattering centers are set to $P_{\text{near}} = 0.6$, $P_{\text{far}} = 0.1$ and $P_{\text{interior}} = 0.3$, which is more similar to those

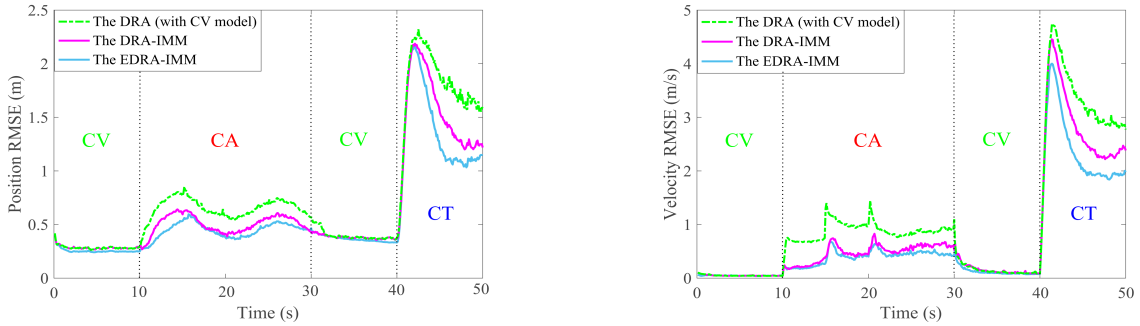


(a) Position RMSE. (b) Velocity RMSE.

Fig. 6. Comparison of the RMSEs of the standard DRA method (using the CV model only), the proposed DRA-IMM and the proposed EDRA-IMM.

TABLE II
PERFORMANCE EVALUATION OF THE PROPOSED METHODS

| | CV Stage (0-10s and 30-40s) | | CA Stage (10-30s) | | CT Stage (40-50s) | |
|---|---|---|---|---|---|---|
| | Pos. RMSE $(m)$ | Vel. RMSE $(m/s)$ | Pos. RMSE $(m)$ | Vel. RMSE $(m/s)$ | Pos. RMSE $(m)$ | Vel. RMSE $(m/s)$ |
| DRA (CV) | 0.33 | 0.10 | 0.65 | 0.88 | 1.78 | 3.29 |
| **DRA-IMM** | 0.34 | 0.11 | 0.50 | 0.48 | 1.52 | 2.79 |
| **EDRA-IMM** | 0.31 | 0.08 | 0.45 | 0.40 | 1.35 | 2.34 |

of the real dataset like nuScenes [22]. The sampling interval is $0.1s$. The covariance matrices of process noise in different models are set by

$$\begin{aligned}\mathbf{Q}^{CV} &= \mathbf{Q}^{CA} = \mathrm{diag}\left(\left[0.1^2, 0.1^2, 10^{-6}, 10^{-4}\mathbf{I}_4\right]\right)\\ \mathbf{Q}^{CT} &= \mathrm{diag}\left(\left[0.5^2, 0.5^2, 10^{-6}, 10^{-4}\mathbf{I}_4\right]\right).\end{aligned} \tag{42}$$

The covariance matrix of measurement noise is set by

$$\mathbf{R} = \mathrm{diag}\left(\left[0.1^2, 0.027^2, 0.005^2\right]\right). \tag{43}$$

The measurement data is generated with the extension model in Section III-B, while the ground truth of target motion model and vehicle shape can be used (in contrast to the estimated value for tracking).

The proposed DRA-IMM and EDRA-IMM are compared with the standard DRA in terms of the root-mean-square error (RMSE) in position and in velocity. Fig. 5 displays the estimated probabilities of the CV, CA, and CT models of the proposed DRA-IMM. The intervals with different background colors correspond to different target motion models. The motion model with the highest probability estimated by the proposed DRA-IMM is highly consistent with the truth, and the estimated model probabilities respond rapidly to the vehicle maneuvers ($10s, 15s, 20s, 30s$ and $40s$), which verifies that the proposed DRA-IMM can precisely estimate the probabilities of the motion models.

The RMSEs of the standard DRA using CV model and the proposed DRA-IMM over 1000 Monte Carlo are plotted in Fig. 6. The RMSE of the standard DRA is low only when the target performs CV motion, but rises dramatically when the target vehicle maneuvers. In contrast, the proposed DRA-IMM method yields lower RMSE than the standard DRA, and maintains much better robustness in case of vehicle maneuvers. From Table II, the RMSE of the proposed DRA-IMM is reduced by approximately 23% in position and 45% in velocity during CA motion, and by about 15% in both position and velocity during CT motion over the standard DRA. Furthermore, the proposed DRA-IMM yields a lower peak RMSE than the standard DRA when the target executes maneuvers. It is concluded that the proposed DRA-IMM achieves more satisfying estimation performance than the standard DRA.

Fig. 6 also validates the further improvement of the proposed EDRA-IMM over the basic DRA-IMM. It is shown that when the target performs maneuvering motion, the RMSE of the proposed EDRA-IMM is lower than that of the DRA-IMM. The RMSE of the proposed EDRA-IMM is reduced by about 11% in position and 17% in velocity during CA motion, and by 11% in position and 16 % in velocity during CT motion compared to the DRA-IMM. This is due to the fact that the basic DRA-IMM ignores the correlation between the vehicle extension and its kinematic state, and uses a constant prior data-region association probability. In contrast, the proposed EDRA-IMM implements a ray-based strategy to calculate the prior data-region association probability in real time and in accordance with the estimated kinematic state. Accordingly, the proposed EDRA-IMM is superior to the basic DRA-IMM especially when the target maneuvers.

## V. CONCLUSION

In this paper, we first propose a novel DRA-IMM method for maneuvering extended vehicle tracking with automotive radar. The proposed DRA-IMM method achieves better robustness in case of vehicle maneuvers than the standard DRA

method. Based on that, an EDRA-IMM method, characterized by a ray-based approach, is proposed. The EDRA-IMM efficiently extracts the prior information of data-region association from the estimated kinematic state and thus further improves the tracking performance, especially when the target vehicle maneuvers. Simulation result validates the superiorities of the proposed methods in robustness over the standard DRA, along with the further improvement of the proposed EDRA-IMM over the basic DRA-IMM. In our future work, real-world radar data will be used to further improve the proposed methods.

## REFERENCES


[1] M. Feldmann, D. Fränken, and W. Koch, "Tracking of extended objects and group targets using random matrices," *IEEE Transactions on Signal Processing*, vol. 59, no. 4, pp. 1409–1420, 2010.

[2] J. Lan and X. R. Li, "Tracking of maneuvering non-ellipsoidal extended object or target group using random matrix," *IEEE Transactions on Signal Processing*, vol. 62, no. 9, pp. 2450–2463, 2014.

[3] M. Baum, B. Noack, and U. D. Hanebeck, "Extended object and group tracking with elliptic random hypersurface models," in *2010 13th International Conference on Information Fusion*, 2010, pp. 1–8.

[4] M. Baum and U. D. Hanebeck, "Shape tracking of extended objects and group targets with star-convex rhms," in *14th International Conference on Information Fusion*, 2011, pp. 1–8.

[5] X. Cao, J. Lan, X. R. Li, and Y. Liu, "Automotive radar-based vehicle tracking using data-region association," *IEEE Transactions on Intelligent Transportation Systems*, 2021.

[6] M. Buhren and B. Yang, "Simulation of automotive radar target lists using a novel approach of object representation," in *2006 IEEE Intelligent Vehicles Symposium*, 2006, pp. 314–319.

[7] Y. Li, G. Li, Y. Liu, X.-P. Zhang, and Y. He, "A novel smooth variable structure filter for target tracking under model uncertainty," *IEEE Transactions on Intelligent Transportation Systems*, vol. 23, pp. 5823–5839, 2022.

[8] Y. Li, G. Li, Y. Liu, X.-P. Zhang, and Y. He, "A hybrid svsf algorithm for automotive radar tracking," *IEEE Transactions on Intelligent Transportation Systems*, vol. 23, pp. 15 028–15 042, 2022.

[9] Y. Li, G. Li, Y. Liu, X.-P. Zhang, and Y. He, "Statically fused smooth variable structure filter for robust tracking with doppler radar," in *2022 IEEE Radar Conference (RadarConf22)*. IEEE, 2022, pp. 1–6.

[10] X. Rong Li and V. Jilkov, "Survey of maneuvering target tracking. Part I. dynamic models," *IEEE Transactions on Aerospace and Electronic Systems*, vol. 39, no. 4, pp. 1333–1364, 2003.

[11] X. R. Li and V. P. Jilkov, "Survey of maneuvering target tracking: Part II. ballistic target models," in *Signal and Data Processing of Small Targets 2001*, vol. 4473, 2001, pp. 559–581.

[12] X. R. Li and V. P. Jilkov, "Survey of maneuvering target tracking: Part III. measurement models," in *Signal and Data Processing of Small Targets 2001*, vol. 4473, 2001, pp. 423–446.

[13] X. R. Li and V. P. Jilkov, "Survey of maneuvering target tracking. Part V. multiple-model methods," *IEEE Transactions on Aerospace and Electronic Systems*, vol. 41, no. 4, pp. 1255–1321, 2005.

[14] X. R. Li and V. P. Jilkov, "A survey of maneuvering target tracking: Part IV: Decision-based methods," *Proceedings of SPIE - The International Society for Optical Engineering*, vol. 4728, 2002.

[15] Y. Bar-Shalom, T. E. Fortmann, and P. G. Cable, "Tracking and data association," *Acoustical Society of America Journal*, vol. 87, no. 2, pp. 918–919, 1990.

[16] E. Mazor, A. Averbuch, Y. Bar-Shalom, and J. Dayan, "Interacting multiple model methods in target tracking: a survey," *IEEE Transactions on Aerospace and Electronic Systems*, vol. 34, no. 1, pp. 103–123, 1998.

[17] Y. Bar-Shalom, X. R. Li, and T. Kirubarajan, *Estimation with applications to tracking and navigation: theory algorithms and software*. John Wiley & Sons, 2004, pp. 179–198.

[18] M. R. Morelande and N. J. Gordon, "Target tracking through a coordinated turn," in *Proceedings.(ICASSP'05). IEEE International Conference on Acoustics, Speech, and Signal Processing, 2005.*, vol. 4, 2005, pp. 21–24.

[19] C. Knill, A. Scheel, and K. Dietmayer, "A direct scattering model for tracking vehicles with high-resolution radars," in *2016 IEEE Intelligent Vehicles Symposium (IV)*, 2016, pp. 298–303.

[20] S. J. Julier and J. K. Uhlmann, "Unscented filtering and nonlinear estimation," *Proceedings of the IEEE*, vol. 92, no. 3, pp. 401–422, 2004.

[21] A. Petrovskaya and S. Thrun, "Model based vehicle detection and tracking for autonomous urban driving," *Autonomous Robots*, vol. 26, no. 2, pp. 123–139, 2009.

[22] H. Caesar, V. Bankiti, A. H. Lang, S. Vora, V. E. Liong, Q. Xu, A. Krishnan, Y. Pan, G. Baldan, and O. Beijbom, "nuscenes: A multimodal dataset for autonomous driving," in *Proceedings of the IEEE/CVF conference on computer vision and pattern recognition*, 2020, pp. 11 621–11 631.